Oceanographic indicators for Northern shortfin squid (*Illex illecebrocus*) in the Northwest Atlantic

A Working Paper for consideration by the

2021 Illex Research Track Assessment Working Group

Sarah L. Salois, Kimberly J. W. Hyde, Adrienne M. Silver, Avijit Gangopadhyay, Glen Gawarkiewicz, Anna Mercer, Brooke Lowman, John Manderson, Paul Rago

21 January 2022

Introduction

Oceanographic satellite imagery provides a powerful tool for assessing dynamic marine systems in a rapidly changing ocean. Remotely sensed data are well suited for environmental analysis and ecological forecasting as they provide long-term synoptic, near real-time coverage of oceanographic conditions at high spatial (1-4 km) and temporal (daily) resolutions. This work utilizes these long term time series, as well as global ocean reanalysis physical data, to generate high resolution metrics to serve as potential indicators for understanding the distribution and availability of the commercially important northern shortfin squid, *Illex illecebrosus*. Recent years have seen above average availability to the U.S. fishery, yet the drivers associated with the high abundance years are unknown. It is thought that variable population dynamics exhibited by *Illex* in the U.S. Mid-Atlantic fishery are largely influenced by oceanographic conditions of the Northwest Atlantic (Dawe et al. 2007, Hendrickson 2004, Hendrickson and Holmes 2004), which have documented significant changes over the past decade (Gangopadhyay et al. 2019, Gonçalves Neto et al. 2021, Seidov et al. 2021, Silver et al. 2021).

The purpose of this working paper is to investigate a suite of oceanographic features (e.g.: mesoscale eddies, fronts) to assess and characterize their relationships to *Illex* catch rates. To achieve this goal, we collaborated with a multi-disciplinary group of experts across government, academia, and industry to generate a series of hypotheses linking oceanographic features to potential mechanisms driving both the ingress and egress of *Illex* to the southern stock component of the fishery. The following five general hypotheses informed the selection and spatial scale of covariates considered in the multivariate statistical models used in this study.

(i) Frontal dynamics may create areas of high productivity (implications for abundance/distribution/growth/aggregation)

(ii) Warm core rings may serve as a transport/retention mechanism for larval stage/pre-recruits (implications for immigration, mortality, emigration)

(iii) Strength and location of warm core rings may contribute to increased primary productivity due to upwelling of nutrients and provide a mechanism to concentrate food sources for juveniles and adults (implications for aggregation, abundance, growth, distribution)

(iv) Bottom temperature may influence (optimal) habitat selection for managing metabolic demands of juveniles and adults (implications for emigration, growth, aggregation)

(v) Changes in slope water composition may have profound impacts on *Illex* distribution (implications for immigration/emigration)

The identification of oceanographic drivers of *Illex* catch in space and time is an important first step in increasing our understanding around the mechanistic processes influencing the availability of *Illex* on the northeast US continental shelf. Understanding the movement of this species into and out of the ecosystem and fishery is highly relevant in reaching future stock assessment and management goals for *Illex*.

Methods

Fishery dependent catch data

This study uses estimates of the nominal *Illex* catch per unit effort (CPUE) calculated from two high resolution datasets maintained by the Northeast Fishery Science Center's (NEFSC) Study Fleet program and Observer program from 2008-2020. The CPUE estimates used for this study were derived by Lowman and colleagues (2021) and resulting values were summed across weeks and fishing locations. The Observer data consists of catch data collected onboard commercial fishing vessels by professionally trained biologists (observers) at the tow level. The Study Fleet data is voluntary self-reported catch and effort data from individual tows collected by captains on participating vessels. The Observer data is collected from approximately 10% of the *Illex* fishing trips annually, with lower coverage rates in recent years. The Study Fleet data is collected from approximately ~ 40% of fishing trips annually, with higher coverage in recent years. The Study Fleet and observer datasets were for this study due to their fine scale spatiotemporal data on *Illex* catch and effort, which is required for exploring potential oceanographic indicators. Specifically, these datasets include detailed fishing trip location start and end points via GPS coordinates (see Lowman et al. 2021a, b and Jones et al. 2020 for more dataset specifics), which was instrumental in identifying co-located environmental conditions.

Models run in this study utilize catch from both 'targeted' and 'untargeted' trips, in effort to reduce the biases implicit in using fishery dependent catch and effort data as an index of abundance. Combining all available tow data where catch comprises greater than 10% *Illex* (and more than 100 pounds landed), previously described as the 'comprehensive data set' by Jones and colleagues (2020), allowed for the examination of a larger number of trips over a greater range of space and time and the ability to capture instances of both low and high catch throughout the region.

The resulting catch data was subset into two fishing fleets based on vessel hold type (Freezer Trawlers and 'Wet Boats'). This decision follows work by Lowman and colleagues (2021) as well as correspondence via *Illex* Working Group meetings and industry conversations, where clear differences in fishing behavior and capacity were noted between fleets (Mercer et al. 2022). These differences stem from the highly perishable nature of this species and differential processing capacity of the two fleet types (Mercer et al. 2022, Lowman et al. 2021b). The particular set of constraints imposed by 'wet boats' makes them more likely to reflect real-time responses to oceanographic conditions and more likely to pick up an environmental signal as opposed to freezer trawlers which have a 'ceiling' or limit to the amount of squid they can take on board, even during instances of high squid availability. Therefore, only wet boats (vessels

with refrigerated sea water or ice holds) were considered for this study, excluding all freezer trawlers.

Oceanographic Covariate Data

The majority of the environmental covariates were either direct observations via remotely sensed satellite data or metrics derived from remote sensed products. Satellite remote sensors are an ideal data source for assessing dynamic marine ecosystems because they provide long-term synoptic, near real-time coverage of near-surface oceanographic conditions at high spatial (1-4 km) and temporal (daily) resolutions. To understand subsurface conditions, weekly bottom temperature and salinity time series were derived from a daily GLORYS12V1 global ocean reanalysis model data (CHEMS, 2018) that was subset over the northwest Atlantic and averaged to create weekly products. This modeled product has a gridded 8-km horizontal resolution, up to 50 fixed vertical depth bins, and the data are available from 1993 to 2020.

Remote sensing data

Daily Level 3 (L3) mapped (4km resolution, sinusoidally projected) satellite ocean color data (version 5.0; Sathyendranath et al, 2021) were obtained from the European Space Agency's Ocean Colour Climate Change Initiative (OC-CCI) project (Sathyendranath et al., 2019). The OC-CCI dataset comprises of globally merged SeaWIFS, MERIS, MODIS-Aqua, VIIRS and Sentinel3A-OLCI data. The L3 OC-CCI products include chlorophyll a (CHL-CCI), remote sensing reflectance (Rrs(λ)), and several inherent optical property products (IOPs). The CHL-CCI blended algorithm attempts to weight the outputs of the best-performing chlorophyll algorithms based on the water types present, which improves performance in nearshore water compared to open-ocean algorithms.

Daily sea surface temperature (SST) data (gridded 1km resolution) were acquired from the Group for High Resolution Sea Surface Temperature (GHRSST) Multiscale Ultrahigh Resolution (MUR, version 4.1) Level 4 (L4) data (JPL MUR MEaSUREs Project, 2015). The MUR analysis ingests the Moderate Resolution Imaging Spectroradiometer (MODIS) retrievals and seeks to capture small scale SST structures wherever available. The MODIS data are combined with lower resolution SST data from satellite infra-red and microwave sensors as well as *in situ* measurements (Chin et al. 2017).

The global CHL and SST products were spatially subset to the U.S. East Coast (SW longitude=-82.5, SW latitude=22.5, NE longitude=-51.5, NE latitude=48.5). Weekly statistics (minimum, maximum, mean, standard deviation and coefficient of variation) were calculated for both CHL and SST. Climatological weekly means were calculated from the entire time series (1998-2020 for CHL and 2003-2020 for SST) to generate the anomalies. CHL in the NES are log-normally distributed, thus to calculate the CHL anomaly (CHL_{anom}) the data are first log-transformed before taking the difference between the weekly mean (CHL_i) and the climatological mean (CHL_{ci}), which results in a unitless CHL anomaly ratio (Eq 1.).

$$CHL_{anom} = EXP(\log_{ln}(CHL_i) - \log_{ln}(CHL_{ci})) \quad \text{(Eq 1.)}$$

The SST anomaly (SST_{anom}) is just the difference between the weekly SST (SST_i) and the climatological mean (SST_{ci}) (Eq 2.).

$$SST_{anom} = SST_i - SST_{ci} \quad \text{(Eq 2.)}$$

Oceanographic fronts

Oceanographic fronts are narrow zones of enhanced horizontal gradients of water properties (temperature, salinity, chlorophyll, etc.) that represent major biogeographical/ecosystem boundaries and are often associated with zones of elevated primary and secondary productivity and can be "hot spots" of marine life and fishing (Belkin et al., 2009). For the frontal data, daily high resolution (1km) MODIS imagery from the Aqua and Terra satellites were acquired from the NASA Ocean Biology Processing Group (OBPG). The Level 1A MODIS-Aqua ocean color files (NASA, 2018) were processed using the NASA Ocean Biology Processing Group SeaDAS software version 7.4. All MODIS imagery were spatially subset to the U.S. East Coast (SW longitude=-82.5, SW latitude=22.5, NE longitude=-51.5, NE latitude=48.5) using L1AEXTRACT_MODIS. SeaDAS's L2GEN program was used to generate Level 2 (L2) products including chlorophyll a (CHL) using the default settings and optimal ancillary files. MODIS-Aqua SST (4µm night and 11µm day images; NASA, 2019) and MODIS-Terra CHL (NASA, 2018) and SST (4µm night and 11µm day images; NASA, 2019) were downloaded from OBPG as L2 files. The SeaDAS L2BIN program spatially and temporally aggregated the L2 files to create daily Level 3 binned (L3B) files. The daily files were binned at 2 km resolution that are stored in a global, nearly equal-area, integerized sinusoidal grids and the CHL files use the default L2 ocean color flag mask.

Daily CHL and SST frontal gradients were calculated using the Belkin and O'Reilly (2009) algorithm. CHL fronts are more diverse and complex than SST fronts and thus this algorithm uses a contextual median filter to preserve the main features of the CHL field, namely CHL enhancement on hydrographic fronts and CHL blooms. Prior to running the algorithm, the CHL data were log-normally transformed to account for the log-normal distribution of CHL. Because the gradient data are normalized differences between pixels, data from the Aqua and Terra sensors were merged into daily files, which were then used to create weekly frontal metrics.

Derivation of frontal metrics

In order to isolate prominent frontal features, a threshold of 0.4°C (SST) and 0.06 mgm^{-3}(CHL) was applied to the frontal gradient data (Miller 2009, Suberg et al. 2019). Following methods by Suberg et al. (2019), the number of valid frontal pixels (*Fvalid*) was identified for each satellite image and summed across a seven-day period. The metric calculated by summing the number of times a pixel exceeded the frontal threshold in a given week. For example, if a pixel was identified as frontal on days 1, 3, 4, and 5 of a given week, it would have a *Fvalid* value of 4. This metric was used as a covariate for this study by determining the proportion of valid frontal pixels in a given area per week (see Table 1 and Figure 1 for details on areas of data extraction).

Warm core rings

Warm core rings (WCRs) are anti-cyclonic mesoscale eddies that break off from the Gulf Stream (GS), after it detaches from the coast around Cape Hatteras. Once detached from the stream, these mesoscale eddies move in a west-southwestward direction carrying the entrapped warm GS water through the slope sea to the US continental shelf region (Gangopadhyay et al., 2020; Silva

et al. 2021). When a WCR impinges on the shelf slope, its inherent anticyclonic properties (clockwise movement of surface waters) create differential water characteristics on opposing sides of the ring (Morgan and Bishop, 1977; Gawarkiewicz et al., 2001; Cenedese et al., 2013). On the eastern edge of the ring, cooler shelf water is entrained and exported from the shelf into the slope sea creating a streamer of shelf water (Gawarkiewicz et al., 2001). These shelf water streamers may interact with the Middle Atlantic Bight (MAB) Shelfbreak Jet resulting in an area of increased upwelling (Ryan et al., 1999; Forsyth et al. 2020; Forsyth et al., 2021). Conversely on the western edge of the ring, there is a steepening of the shelfbreak front combined with an onshore flow, resulting in warmer, more saline water intrusions (Gawarkiewicz et al., 2001). Recent years have seen a significant increase in the number and frequency of these mesoscale eddies (Gangopadhyay et al., 2019) which potentially play a key role in the changing dynamics of the Northwest Atlantic shelf and slope waters (Gawarkiewicz et al., 2018; Harden et al., 2020; Chen et al., 2021; Gawarkiewicz et al., 2022).

Derivation of warm core ring metrics

(i) Ring tracking census

A Gulf Stream ring tracking dataset of weekly ring size and location was generated from Jenifer Clark's Gulf Stream Charts for the years 2011 through 2020. These charts have been previously used to create a 38 year WCR census (Gangopadhyay et al., 2019 and 2020). Following the same methodology as Gangopadhyay et al. (2020), location and ring area were verified using a QGIS framework. Several different ring indices were created from this dataset.

(ii) Ring occupancy

Ring Occupancy is an index created to calculate the number of "ring days" on the Northeast continental shelf. A ring was considered to 'occupy the shelf' if the approximate radius (calculated from ring area assuming the ring was a perfect circle) was longer than or equal to the distance from the ring center to the nearest point of the 100m isobath. The number of ring days was calculated by combining the total number of rings on the shelf and the number of days they remained there. For example, in a given week, if ring A spends 3 days on the shelf, and ring B spends 7 days on the shelf, the ring occupancy would be equal to 10 (ring days). This index was calculated on weekly, monthly and annual time scales.

(iii) Ring Footprint Index

The Ring Footprint Index (RFI) accounts for both the amount of time a ring spends in a given area as well as its size, where: RFI = ring days per ring area / (total area of region * total time period). This index was adapted from the RFI calculated in Gangopadhyay et al. (2020). The numerator, ring days per ring area, multiplies the time a ring is in a given region (zone) by the area of the ring. This term is then divided by a second term, which multiplies the total area of the zone by the total time period of interest. This was calculated at a weekly time scale across 4 different longitudinal zones binned by 5° increments (Zone 1: 75-70°W, Zone 2: 70-65°W, Zone 3: 65-60°W, and Zone 4: 60-55°W, see Figure 2).

(iiv) Ring Orientation

Ring Orientation is a metric derived in effort to better understand the relationship between the physical properties of warm core rings and catch locations. Information about the ring angle accounts for (i) the processes that are related to the presence of the ring and (ii) the orientation of the ring traveling past a fishing point. This ring orientation metric was calculated by identifying ring and fishing location reference points and calculating the angle between them (Fig. 3). Specifically, coordinates detailing each ring's northern, western, eastern, southern and center

points as well as the location where the ring meets the 100 meter isobath were identified. This series of coordinates was then paired with fishing locations and used to generate two lines and their associated angles (Fig. 3). Comparison between resulting angles was used to determine the orientation of a given ring to individual fishing locations. For a given week, we calculated the distance between individual fishing points and all rings present. Ring orientation was then calculated between a given fishing point and the closest ring associated with that location.

Generalized Additive Modeling

To examine relationships between *Illex* CPUE and oceanographic covariates, we fit generalized additive models (GAMs) to the combined Study Fleet and Observer datasets. GAMs are a powerful statistical tool and are increasingly used in ecological contexts as they are inherently flexible and thus able to account for nonlinear relationships without compromising interpretability (Pederson et al., 2019). This flexibility stems from the additive framework of GAMs, which uses local smoothing functions to fit predictor variables to a response variable. Here, the response variable (CPUE) was adjusted via a negative binomial error distribution with a log link function to account for positive skew and over dispersion. Explanatory variables consisted of thirty-one candidate oceanographic metrics across multiple spatial scales (Table 1). A strength of GAMs is their ability to account for relationships between variables occurring on different scales. We facilitated regular correspondence among experts in the fishing industry, oceanography, fisheries, and management to generate a series of hypotheses describing potential relationships between *Illex* catch and key oceanographic processes. These hypotheses were used to inform and select the spatial scale at which each oceanographic dataset was extracted. GAMs were fit using an iterative variable selection process and the optimal model was chosen based on lowest Akaike Information Criterion (Burnham & Anderson, 2002) and highest deviance explained as in similar work from these datasets by Jones et al. (2020) and Lowman et al. (2021), for consistency. All GAMs were run in R 4.0.5 (R Core Team, 2021) using the *mgcv* package (Wood, 2011).

Results

Generalized Additive Modeling

Generalized additive model results identified ten covariates that were significant predictors of *Illex* catch-per-unit-effort, including temporal (year, week), spatial (latitude, longitude, and NAFO subareas) and environmental (bottom temperature, ring footprint index, ring orientation, salinity at the 222 meter isobath, chlorophyll frontal activity, and standard deviation in sea surface temperature) variables (Table 1, Fig. 4). The full model accounted for 69.9 % of the deviance explained. The main temporal trends that emerged in the full model are consistent with findings from Jones and colleagues (2020) as well as Lowman and colleagues (2021), where catch is relatively stable in the beginning of the time series (2011, 2012) experiences a significant drop in year 2013 followed by three consecutive low years (2014, 2015, 2016) and significantly higher catch over the most recent four years (2017, 2018, 2019, 2020, Fig. 4h). The spatial smoother captured the interacting effects of latitude and longitude and identified hot spots of catch along the shelf break (Fig.4a). Fishing locations were categorized by Northwest Atlantic Fisheries Organization (NAFO) subareas, which identified differences in catch between Northern and Southern portions of the southern stock component (Table 2, Fig. 4k).

The ecological predictors revealed some interesting patterns. The most impactful ecological predictor in this analysis was bottom water temperature. Its effects suggest a small range of cooler bottom temperatures (6-10°C) support higher catch with a peak around 6.5°C (Fig. 4b). Salinity at 222 meters exhibits a multi-modal relationship between salinity and catch with two smaller peaks at 35.45 and a larger peak at 35.73 psu (Fig. 4c). Important mesoscale features included the presence of rings in the slope sea between 70 and 65°W longitude (i.e. Zone 2), 6 months prior to catch, and Zone 1(between 75-70°W), 3 months prior to catch. Specifically, in a given week, the highest catch was associated with a ring footprint index of 0.3 (Fig. 4de). Additionally, there was a significant positive effect of ring orientation on *Illex* catch, where fishing locations on the eastern side of rings had significantly higher catch than fishing locations on the western side of a particular warm core ring (Fig. 4j). There was a bi-modal relationship between catch and the variability in sea surface temperature with peaks at standard deviation values of 0.4 and 0.9, suggesting higher catch associated with more variable surface temperature conditions (Fig. 4f). Finally, chlorophyll frontal dynamics in fishing areas (i.e. the proportion of area identified as a chlorophyll front) revealed higher catch when greater than 40% of the area is identified as chlorophyll fronts (Fig. 4g).

Discussion/Research Recommendations

The results from this study largely support the hypotheses developed by the multidisciplinary research team and industry collaborators. In particular, results suggest a suite of environmental variables which may serve as indicators of *Illex* habitat condition or areas of increased primary productivity. These indicators are of interest due to their implications for identifying potential areas of *Illex* aggregation and better understanding their distribution and availability to the fishery. In particular, bottom temperature and ring footprint index may be useful indicators for habitat conditions relevant to *Illex* juvenile/adult and pre-recruit/larval life stages, respectively, whereas the remaining covariates, ring orientation, salinity, and chlorophyll frontal dynamics are potential indicators of areas of high productivity. Results from GAMs identified low mean bottom temperatures as a strong predictor of CPUE, which is consistent with results from surveys done by Hendrickson (2004), where juveniles were associated with deeper waters (140 - 260m) and lower bottom temperatures (9.9 ℃). Existing hypotheses around habitat conditions explaining the relationship between *Illex* occurrence and cooler bottom temperatures have been attributed to both the selection of cooler temperatures to manage metabolic demands and the use of depth to avoid predation (Benoit-Bird and Moline, 2021). Bottom temperatures on the shelf are highly dependent on local processes (e.g.: circulation and intrusions) and variable in space and time (Chen et al., 2021), therefore more research is needed to better understand this relationship. The lagged ring footprint index, a measure of ring occupancy in the slope sea, may serve as an additional indicator of habitat condition for pre-recruit/larval stages. Examining ring footprints in the slope sea at 6 and 3-month lag times was an effort to (i) understand slope water conditions in areas previously identified as important for larval stages of the *Illex* (Bakun and Csirke, 1998; Dawe et al., 2007), and (ii) gain insight into rings as potential transport/retention mechanisms. The significant relationship that emerged between catch and a lagged WCR footprint index in slope sea zones (higher catch at RFI > 0.3 in zone 2 lagged by 6 months, see Figure 4c), is an important result that merits further investigation as it may have implications as a pre-season indicator. Recent research conducted by Jones and Hendrickson, to address TOR 3, has identified two predominant *Illex* cohorts, with one cohort hatching in the winter and one

cohort hatching in the summer, with specific hatch times varying inter-annually (Jones and Hendrickson, *unpublished manuscript*). This work extends the findings of Hendrickson (2004) that a winter cohort supports the *Illex* fishery to include a summer cohort that supports the latter part of the fishery. Thus, having an indication of the total area of the slope sea occupied by WCRs during the winter hatch months (January - March) may provide greater understanding of the habitat conditions (salinity, temperature, productivity) under which newly hatched *Illex* are exposed. Increased characterization of the presence and timing of mesoscale oceanographic features in areas occupied by newly hatched *Illex* may also provide insight into the habitat characteristics that are favorable to newly hatched *Illex*, which has the potential to improve our ability to forward-project availability of mature squid to the fishery.

The remaining covariates can be summed up as indicators of areas of high productivity. Namely, the significance of the eastern orientation of a warm core ring to a fishing point supports our hypotheses that that *Illex* abundance is likely to be higher or more concentrated on the eastern edge of a warm core ring. Specifically, Forsyth and colleagues (2021) have found that as a WCR impinges on the shelf, the interaction between the shelf streamer created on its eastern edge and the MAB Shelfbreak Jet can result in increased upwelling (by a factor of ten) resulting in enhanced productivity in those locations (Forsyth et al., 2020; Gawarkiewicz et al., 2001; Cenedese et al., 2013). Additionally, the strong significant relationship between high catch and sub-surface salinity greater than 35.6 psu (at 222 meters depth) is also an important and informative indicator of productivity, and indicates a meaningful relationship between mid-depth intrusions of Gulf Stream water and *Illex* squid. Near surface salinity measurements are less indicative of a warm core ring because surface salinity is more variable due to the mixing of surface waters, whereas higher salinity at a depth of 200 meters is more indicative of the presence of a warm core ring and also coincident with the near-bottom preference of *Illex* squid. Additionally, the 200 meter isobath is roughly the mean position of the MAB Shelfbreak Jet, where upwelling can reach the 26.0 isopycnal. The interaction of the jet and the highly saline ring water has the potential to support high levels of primary productivity (Forsyth et al., 2020; Oliver et al., 2021). The two smaller salinity peaks at 35.3 and 35.4 psu are likely signals of older rings that have mixed with surrounding slope water, characterized by smaller diameters and less vertical extent than rings with higher salinity of 35.7-35.8 psu (Gawarkiewicz et al., 2001; Silva et al., 2020).

The relationship that emerged between higher standard deviations in sea surface temperature and catch is not unexpected as the highest amount of variation in sea surface temperature occurs at the shelf-break front (Linder and Gawarkiewicz, 1998), which is also the location of the majority of the fishing effort. The ecological interpretation of this trend is less clear as the variability in SST may simply be acting as an indicator for capturing heterogeneity in the environment, including bathymetric features (such as high slope). Alternatively, this relationship may serve as a useful indicator of changes in the water composition, where increased standard deviations are related to instances of slope water intrusions onto the shelf. Finally, the peaks in CPUE in areas where 30-50 percent of the surface is identified as chlorophyll fronts support the hypothesis that chlorophyll frontal activity can serve as a near-surface indicator of productivity, with biological implications for benthopelagic species such as *Illex* squid.

While these results are correlative in nature, they have strong implications for understanding the mechanistic drivers of the distribution of *Illex* throughout the fishery in space and time. More research is needed to identify and verify these potential drivers in order to move towards in-season management and pre-season forecasting. Therefore, it is our recommendation that future research should focus on the following primary areas concerning *Illex* availability, growth, and aggregation to address key uncertainties in current stock assessment models. Specific research initiatives should include (i) increased *Illex* sampling efforts throughout the slope sea across multiple life history stages (e.g.: larval, juvenile, adult), (ii) categorization of environmental conditions/dynamics of proposed nursery habitat (slope water composition), (iii) isolation and near-real-time monitoring of the shelf break front position via satellite derived metrics, (iv.) standard and continuous categorization of warm core ring trajectories and other mesoscale features, (v) real-time monitoring of salinity maximum intrusions along shelf break, (vi) identification of *Illex* spawning locations, (vii) cooperative research aboard commercial fishing vessels to quantify *Illex* within and around WCRs during the fishing season, (viii) efforts to support fine scale monitoring (both spatial and temporal) including increased fleet participation in fine scale catch reporting, as well as inclusion of new data fields, such as details around location selection, in order to identify if fishing locations are reflective of fishing behavior (gear restrictions, steepness of slope, [mis]matches in trip length/duration with vessel processing abilities) or patterns in squid distribution (aggregation in areas of high productivity).

This work has important implications for the development and understanding of future stock assessments. Having a better understanding of the role of environmental conditions and the mechanistic oceanographic underpinnings driving the productivity and movement of *Illex* is an invaluable part of its stock assessment and management. Specifically, given that multiple cohorts (winter and summer) are likely supporting the *Illex* fishery (Jones and Hendrickson, *unpublished manuscript*), it is imperative to have clarity around the core oceanographic processes driving the observed ingress and egress events of *Illex* in order to support and account for the open population assumption (citations needed: Manderson/Rago working papers) of this fishery in future stock assessment models.

Acknowledgements

We gratefully acknowledge Sarah Gaichas (NEFSC), Katie Almeida (The Town Dock), Bill Bright, Greg Didomenico (Lund's Fisheries), Jeff Kaelin (Lund's Fisheries), Meghan Lapp (Seafreeze LTD), Jimmy Ruhle (CSF), Lisa Hendrickson (NEFSC), Benjamin Galuardi (GARFO), Daniel Hocking (GARFO), Andrew Jones (NEFSC), Paula Fratantoni (NEFSC) and Steve Lorenz (UMASS-SMAST) for all their valuable contributions to this work.

References

Bakun, A., Csirke, J. 1998. Environmental processes and recruitment variability. FAO fisheries technical paper, 105-124.

Belkin, I. M., P. C. Cornillon, and K. Sherman. 2009. Fronts in Large Marine Ecosystems, Progress in Oceanography, 81(1-4), 223-236, doi:doi: 10.1016/j.pocean.2009.04.015.

Belkin, I. M., & O'Reilly, J. E. 2009. An algorithm for oceanic front detection in chlorophyll and SST satellite imagery. Journal of Marine Systems, 78(3), 319-326.

Benoit-Bird, K. J., & Moline, M. A. 2021. Vertical migration timing illuminates the importance of visual and nonvisual predation pressure in the mesopelagic zone. Limnology and Oceanography.

Burnham KP, Anderson DR. 2002. Model Selection and Multi-Modal Inference: A Practical Information-Theoretic Approach (2nd edn). Springer, New York.

Cenedese, C., Todd, R. E., Gawarkiewicz, G. G., Owens, W. B., & Shcherbina, A. Y. 2013. Offshore transport of shelf waters through interaction of vortices with a shelfbreak current. Journal of physical oceanography, 43(5), 905-919.

Chen, K., Gawarkiewicz, G., & Yang, J. 2021. Mesoscale and Submesoscale Shelf-Ocean Exchanges Initialize an Advective Marine Heatwave. *Journal of Geophysical Research: Oceans*, e2021JC017927.

Chen, Z., Kwon, Y. O., Chen, K., Fratantoni, P., Gawarkiewicz, G., Joyce, T. M., ... & Stock, B. C. 2021. Seasonal prediction of bottom temperature on the northeast US continental shelf. Journal of Geophysical Research: Oceans, 126(5), e2021JC017187.

Chin, Toshio Michael, Jorge Vazquez-Cuervo, and Edward M. Armstrong. 2017a. "A Multi-Scale High-Resolution Analysis of Global Sea Surface Temperature." Remote Sensing of Environment 200: 154–69. https://doi.org/10.1016/j.rse.2017.07.029.

CMEMS. 2018. GLORYS12V1 - Global Ocean Physical Reanalysis Product. Retrieved from E.U. Copernicus Marine Service Information website: https://resources.marine.copernicus.eu/?option=com_csw&view=details&product_id=GLOBAL_REANALYSIS_PHY_001_030

Dawe, E. G., Hendrickson, L. C., Colbourne, E. B., Drinkwater, K. F., & Showell, M. A. 2007. Ocean climate effects on the relative abundance of short-finned (Illex illecebrosus) and long-finned (Loligo pealeii) squid in the northwest Atlantic Ocean. *Fisheries Oceanography*, *16*(4), 303-316.

Forsyth, J., Andres, M., & Gawarkiewicz, G. 2020. Shelfbreak Jet Structure and Variability off New Jersey Using Ship of Opportunity Data From the CMV Oleander. Journal of Geophysical Research: Oceans, 125(9), e2020JC016455.

Forsyth, J., G. Gawarkiewicz, and M. Andres, 2021. The impact of Warm Core Rings on Middle Atlantic Bight Shelf Temperature and Shelbreak Jet Velocity. Journal of Geophysical Research – Oceans, submitted.

Gangopadhyay, A., Gawarkiewicz, G., Silva, E. N. S., Monim, M., & Clark, J. 2019. An observed regime shift in the formation of warm core rings from the Gulf Stream. Scientific reports, *9*(1), 1-9.

Gangopadhyay, A., Gawarkiewicz, G., Silva, E. N. S., Silver, A. M., Monim, M., & Clark, J. 2020. A census of the warm-core rings of the Gulf Stream: 1980–2017. Journal of Geophysical Research: Oceans, 125(8), e2019JC016033.

Gawarkiewicz, G., Bahr, F., Beardsley, R. C., & Brink, K. H. 2001. Interaction of a slope eddy with the shelfbreak front in the Middle Atlantic Bight. Journal of Physical Oceanography, 3*1*(9), 2783-2796.

Gawarkiewicz, G., Todd, R. E., Zhang, W., Partida, J., Gangopadhyay, A., Monim, M. U. H., ... & Dent, M. 2018. The changing nature of shelf-break exchange revealed by the OOI Pioneer Array. Oceanography, 31(1), 60-70.

Gawarkiewicz, G., P. Fratantoni, F. Bahr, and A. Ellertson, 2022. Increasing Frequency of Mid-Depth Salinity Maximum Intrusions in the Middle Atlantic Bight. Journal of Geophysical Research-Oceans, submitted.

Gonçalves Neto, A., Langan, J. A., & Palter, J. B. 2021. Changes in the Gulf Stream preceded rapid warming of the Northwest Atlantic Shelf. Communications Earth & Environment, 2(1), 1-10.

Harden, B. E., Gawarkiewicz, G. G., & Infante, M. 2020. Trends in physical properties at the southern New England shelf break. Journal of Geophysical Research: Oceans, 125(2), e2019JC015784.

Hendrickson, L.C. and Holmes, E.M., 2004. Essential fish habitat source document: northern shortfin squid, Illex illecebrosus , life history and habitat characteristics. NOAA Tech Memo NMFS NE, 191, pp. 36.

Hendrickson, L.C., 2004. Population biology of northern shortfin squid (Illex illecebrosus) in the Northwest Atlantic Ocean and initial documentation of a spawning area. ICES Journal of Marine Science, 61 (2), pp.252-266.

Hendrickson, L.C. and Showell, M.A., 2016. Assessment of Northern shortfin squid (Illex illecebrosus) in Subareas 3+ 4 for 2015. NAFO SCR Doc, 16, pp.34.

Jones, A.W., Lowman, B.L., Manderson, J.M, Mercer, A. 2020. An investigation of fine-scale CPUE for northern shortfin squid (*Illex illecebrosus*) using NEFSC Study Fleet data. Working Paper for the MAFMC Illex Working Group and Science and Statistical Committee.

JPL MUR MEaSUREs Project, 2015. "GHRSST Level 4 MUR Global Foundation Sea Surface Temperature Analysis (V4.1)." CA, USA: NASA PO.DAAC. https://doi.org/10.5067/GHGMR-4FJ04. Last accessed 06/01/2021.

JPL MUR MEaSUREs Project, 2015. "GHRSST Level 4 MUR Global Foundation Sea Surface Temperature Analysis (V4.1)." CA, USA: NASA PO.DAAC. https://doi.org/10.5067/GHGMR-4FJ04. Last accessed 06/01/2021.

Lowman, B. A., Jones, A. W., Pessutti, J. P., Mercer, A. M., Manderson, J. P., & Galuardi, B. (2021). Northern shortfin squid (Illex illecebrosus) fishery footprint on the Northeast US continental shelf.

Lowman, B.L., Jones, A.W., Mercer, A. 2021. Northern shortfin squid landings per unit effort. Working paper for the MAFMC Illex Working Group and Science and Statistical Committee.

Mercer, A.J., Manderson, J.P., Rago, P.J.; Lowman, B., Pessutti, J, Wilson, J., Gianesin, G., Alexander, C., Almeida, K., Amory, M., Clarke, R., Goodwin, G., Kaelin, J., Lapp, M., Mitchell, B., O'Neill, G., Ruhle, J., Reichle, W., Reid, E.; Rochford, E., Ruhle, P., Roderick, M., Ruhle, R., Axelsson, L., Axelsson, S., Goodwin, K., Lackner, H., Bright, B., Sawyer, T., Laughlin, S., Wise, J., Cox, M., Wloch, R., Feeney, D., Welch, S., and Jordan, J. 2022. Technical and economic aspects of northern shortfin squid (Illex illecebrosus) processing and marketing essential for interpreting of fishing effort and catch as indicators of population trend and condition. Working Paper for the 2021 Illex Research Track Stock Assessment.

Miller, P. 2009. Composite front maps for improved visibility of dynamic sea-surface features on cloudy SeaWiFS and AVHRR data. Journal of Marine systems, 78(3), 327-336.

Morgan, C. W., & Bishop, J. M. 1977. An example of Gulf Stream eddy-induced water exchange in the Mid-Atlantic Bight. Journal of Physical Oceanography, 7(3), 472-479.

NASA Goddard Space Flight Center, Ocean Ecology Laboratory, Ocean Biology Processing Group. Moderate-resolution Imaging Spectroradiometer (MODIS) Aqua Sea Surface

Temperature Data; 2019 Reprocessing. NASA OB.DAAC, Greenbelt, MD, USA. Last accessed on 06/01/2021.

NASA Goddard Space Flight Center, Ocean Ecology Laboratory, Ocean Biology Processing Group. Moderate-resolution Imaging Spectroradiometer (MODIS) Terra Ocean Color Data; 2018 Reprocessing. NASA OB.DAAC, Greenbelt, MD, USA. doi: 10.5067/TERRA/MODIS/L2/OC/2018.Last accessed on 06/01/2021.

Linder, C. A., & Gawarkiewicz, G. 1998. A climatology of the shelfbreak front in the Middle Atlantic Bight. Journal of Geophysical Research: Oceans, 103(C9), 18405-18423.

Oliver, H., Zhang, W. G., Smith Jr, W. O., Alatalo, P., Chappell, P. D., Hirzel, A. J., ... & McGillicuddy Jr, D. J. 2021. Diatom Hotspots Driven by Western Boundary Current Instability. Geophysical Research Letters, e2020GL091943.

Pedersen, E. J., Miller, D. L., Simpson, G. L., & Ross, N. 2019. Hierarchical generalized additive models in ecology: an introduction with mgcv. PeerJ, 7, e6876.

R Core Team 2019. R: A Language and Environment for Statistical Computing. R Foundation for Statistical Computing. Vienna, Austria. https://www.R-project.org/

Ryan, J. P., Yoder, J. A., Barth, J. A., & Cornillon, P. C. 1999. Chlorophyll enhancement and mixing associated with meanders of the shelf break front in the Mid-Atlantic Bight. Journal of Geophysical Research: Oceans, 104(C10), 23479-23493.

Sathyendranath, S, Brewin, RJW, Brockmann, C, Brotas, V, Calton, B, Chuprin, A, Cipollini, P, Couto, AB, Dingle, J, Doerffer, R, Donlon, C, Dowell, M, Farman, A, Grant, M, Groom, S, Horseman, A, Jackson, T, Krasemann, H, Lavender, S, Martinez-Vicente, V, Mazeran, C, Mélin, F, Moore, TS, Müller, D, Regner, P, Roy, S, Steele, CJ, Steinmetz, F, Swinton, J, Taberner, M, Thompson, A, Valente, A, Zühlke, M, Brando, VE, Feng, H, Feldman, G, Franz, BA, Frouin, R, Gould, Jr., RW, Hooker, SB, Kahru, M, Kratzer, S, Mitchell, BG, Muller-Karger, F, Sosik, HM, Voss, KJ, Werdell, J, and Platt, T (2019) An ocean-colour time series for use in climate studies: the experience of the Ocean-Colour Climate Change Initiative (OC-CCI). Sensors: 19, 4285. doi:10.3390/s19194285

Sathyendranath, S.; Jackson, T.; Brockmann, C.; Brotas, V.; Calton, B.; Chuprin, A.; Clements, O.; Cipollini, P.; Danne, O.; Dingle, J.; Donlon, C.; Grant, M.; Groom, S.; Krasemann, H.; Lavender, S.; Mazeran, C.; Mélin, F.; Müller, D.; Steinmetz, F.; Valente, A.; Zühlke, M.; Feldman, G.; Franz, B.; Frouin, R.; Werdell, J.; Platt, T. (2021): ESA Ocean Colour Climate Change Initiative (Ocean_Colour_cci): Version 5.0 Data. NERC EDS Centre for Environmental Data Analysis, 19 May 2021. doi:10.5285/1dbe7a109c0244aaad713e078fd3059a. http://dx.doi.org/10.5285/1dbe7a109c0244aaad713e078fd3059a

Seidov, D., Mishonov, A., & Parsons, R. 2021. Recent warming and decadal variability of Gulf of Maine and Slope Water. Limnology and Oceanography, 66(9), 3472-3488.

Silva, E. N. S., Gangopadhyay, A., Fay, G., Welandawe, M. K., Gawarkiewicz, G., Silver, A. M., ... & Clark, J. 2020. A Survival Analysis of the Gulf Stream Warm Core Rings. Journal of Geophysical Research: Oceans, 125(10), e2020JC016507.

Silver, A., Gangopadhyay, A., Gawarkiewicz, G., Taylor, A., & Sanchez-Franks, A. 2021. Forecasting the Gulf Stream Path using buoyancy and wind forcing over the North Atlantic. Journal of Geophysical Research: Oceans, 126(8), e2021JC017614.

Suberg, L. A., Miller, P. I., & Wynn, R. B. 2019. On the use of satellite-derived frontal metrics in time series analyses of shelf-sea fronts, a study of the Celtic Sea. Deep Sea Research Part I: Oceanographic Research Papers, 149, 103033.

Wood, S.N., 2011. Fast stable restricted maximum likelihood and marginal likelihood estimation of semiparametric generalized linear models. Journal of the Royal Statistical Society: Series B (Statistical Methodology), 73(1), pp.3-36.
Wood, S.N., 2017. Generalized additive models: an introduction with R. CRC press.

Tables

Table 1. List of all candidate variables modeled. Columns indicate range of variable in dataset used, spatial scale of aggregation/extraction [Northeast Continental Shelf (NES), Northwest Atlantic Fisheries Organization Subareas (NAFO), Northeast Continental Shelf Break (NESBR), Fishing point location (FP)], and whether the variable was included in the final model as well as if they were added as splines (s) or factors (f).

Variable	Range	Spatial Scale	Included
CPUE	2008 - 2020	74 – 66° W , 35 – 45° N	Yes (response)
Year	2011 - 2020	NES	Yes (f)
Week	18 – 44	NES	Yes (f)
Longitude	74.9 - 66.5	NES	Yes (s)
Latitude	35.9 - 45.5	NES	Yes (s)
CHL anomaly	0.53 - 2.08	NAFO	No (s)
CHL mean	0.35 – 2.11	NAFO	No (s)
CHL std. deviation	0.04 – 1.28	NAFO	No (s)
SST anomaly	-2.50 – 2.28	NAFO	No (s)
SST mean	10.24 – 28.41	NAFO	No (s)
SST std. deviation	0.17 – 1.58	NAFO	Yes (s)
CHL Fvalid	0.00 – 0.72	NESBR	Yes (s)
SST Fvalid	0.00 – 0.30	NESBR	No (s)
Bottom temp	3.75 – 14.04	FP	Yes (s)
Salinity 47m	34.55 – 35.92	NESBR	No (s)
Salinity 55m	33.56 – 36.04	NESBR	No (s)
Salinity 110m	34.86 – 36.05	NESBR	No (s)
Salinity 222m	35.21 – 35.83	NESBR	Yes (s)
Distance to ring (km)	3.45 – 886.68	KM	No (s)
Ring distance to shelf (km)	15.41 – 264.58	KM	No (s)
RFI, Zone 1	0.00 - 0.37	75 – 70° W	No (s)
RFI, Zone 2	0.00 – 0.64	70 – 65° W	No (s)
RFI, Zone 3	0.00 – 0.55	65 – 60° W	No (s)
RFI, Zone 4	0. 00 – 0.45	60 – 55°W	No (s)
RFI, Zone 1, lag 6mo	0.00 – 0.30	75 – 70° W	No (s)
RFI, Zone 2, lag 6mo	0.00 – 0.39	70 – 65° W	Yes (s)
RFI, Zone 3, lag 6mo	0.00 – 0.43	65 – 60° W	No (s)
RFI, Zone 4, lag 6mo	0.00 – 0.58	60 – 55°W	No (s)
RFI, Zone 1, lag 3mo	0.00 – 0.38	75 – 70° W	Yes (s)
RFI, Zone 2, lag 3mo	0.00 – 0.55	70 – 65° W	No (s)
RFI, Zone 3, lag 3mo	0. 00 – 0.43	65 – 60° W	No (s)
RFI, Zone 4, lag 3mo	0. 00 – 0.42	60 – 55°W	No (s)
Shelf occupancy	0.00 – 15.00	NES	No (s)
Shelf_occ_Lag6mo	0.00 – 14.00	NES	No (s)
Ring orientation	West, East	NES	Yes (f)
NAFO subarea	5Ze, 5Zw, 6A, 6B,6C	NAFO	Yes (f)

Table 2. Generalized additive model (GAM) results for final model covariate in relation to catch-per-unit-effort (CPUE). Year and week effects are listed in Appendix 2.

Parametric coefficients	Estimate	Std. Error	z-value	p-value
Intercept	6.82321	0.09734	70.096	< 0.001
orientation_E	0.24881	0.01438	17.306	< 0.001
nafo_5zw	-0.03275	0.05929	-0.552	< 0.001
nafo_6a	-0.74700	0.08351	-8.945	< 0.001
nafo_6b	-1.50859	0.08423	-17.911	< 0.001
nafo_6c	-1.77094	0.12805	-13.830	< 0.001
Smooth terms	edf	Ref.df	Chi.sq	p-value
s(lon, lat)	23.927	23.999	52952	< 0.001
s(bt)	8.895	9.000	2325	< 0.001
s(sal_222m)	8.983	9.000	3413	< 0.001
s(z2_lag6mo)	8.976	9.000	4752	< 0.001
s(z1_lag3mo)	8.994	9.000	3928	< 0.001
s(sst_sd)	8.804	8.988	1429	< 0.001
s(fvalid_chl)	8.964	9.000	1452	< 0.001

Figures

Figure 1. Map of Northeast U.S. Continental Shelf Large Marine Ecosystem (NES LME). The colored boxes indicate the bounds of the NAFO subareas. The inner black boundary within NAFO subareas outlines the Northeast Shelf Break (NESBR) region which extends 40 km on either side of the 200 meter isobath. The 200 meter isobath is the brown line within the NESBR region. Zone indicates a given region from which the Ring Footprint Index (RFI) was derived and are longitudinal zones binned by 5 ° increments (Zone 1: 75 -70 °W, Zone 2: 70-65 °W, Zone 3: 65-60 °W, Zone 460-55 °W).

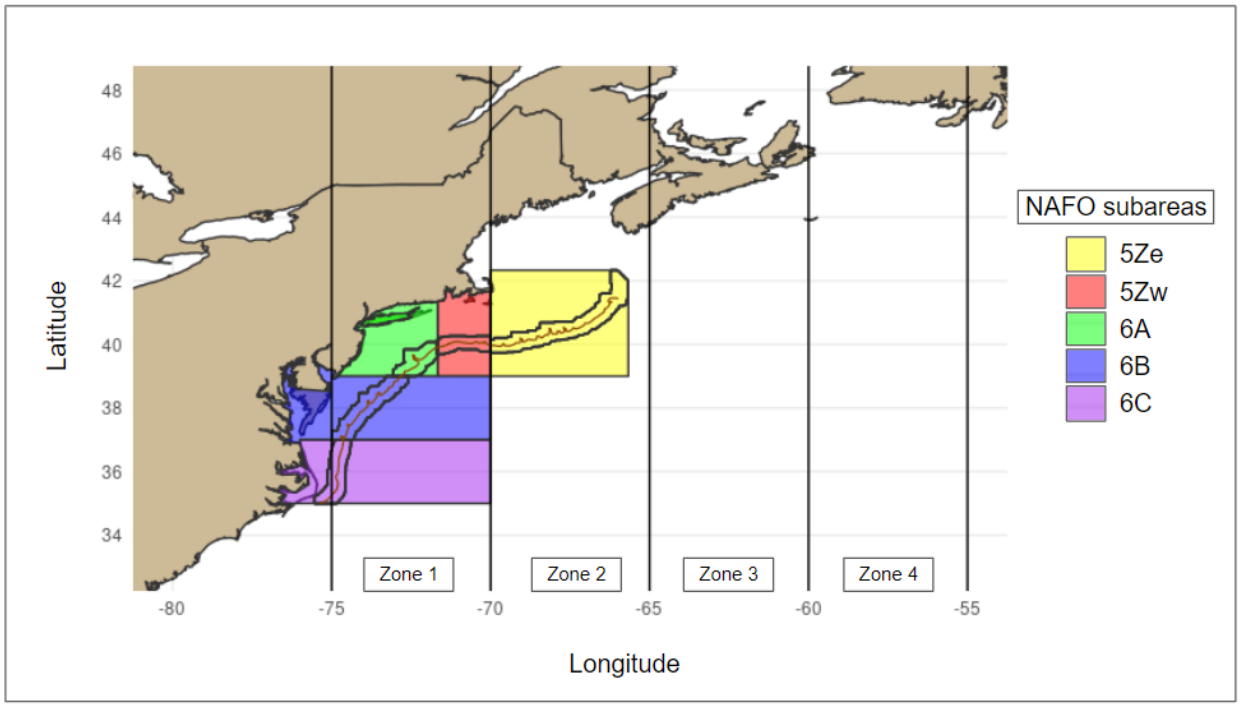

Figure 2. Heat map of Ring Footprint Index (RFI). The yellow arrow indicates the Gulf Stream mean North Wall location. The color bar represents the number of ring days in 0.1 degree bins ranging from 0 to 200. Each panel represents the region (zone) from which the RFI was derived, where (a.) Zone 1, 75 - 70 °W, (b.) Zone 2, 70-65 °W, (c.) Zone 3: 65-60 °W, and (d.) Zone 4, 60-55 °W.

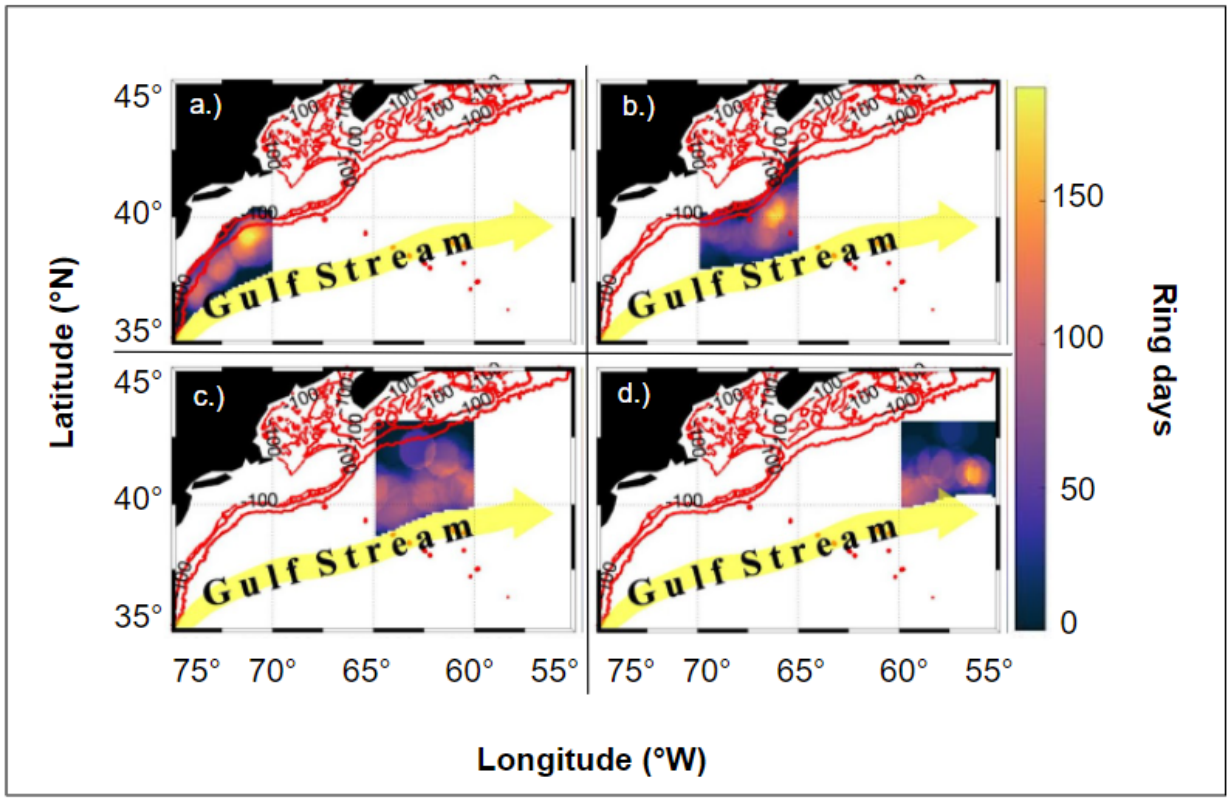

Figure 3. Depiction of warm core ring impingement on the shelf slope and derivation of ring orientation. The bathymetry line is the 100 meter isobath. The circle in the map represents a warm core ring. The reference points on the ring are (T = the location where the ring meets the 100 meter isobath, C = center of point of ring, E = Eastern point of ring). The black triangles outlined in orange (F) indicate fishing point locations. The Eastern side of the ring is indicated by the green shaded area and is associated with offshore transport processes that lead to upwelling. The Western side of the ring is indicated by the blue shaded area and is associated with onshore intrusions. The lines TC and CE represent the ring location in relation to the shelf and form the angle theta (TCE, θ). Lines FC, CE detail the relation between fishing point location and ring, and form the angle, alpha (FCE, α). When alpha (α, FCE) was greater than theta (θ, TCE), the ring was oriented West of the fishing point. Conversely, when angle alpha (α) was less than angle theta (θ), the ring was oriented East of the fishing point.

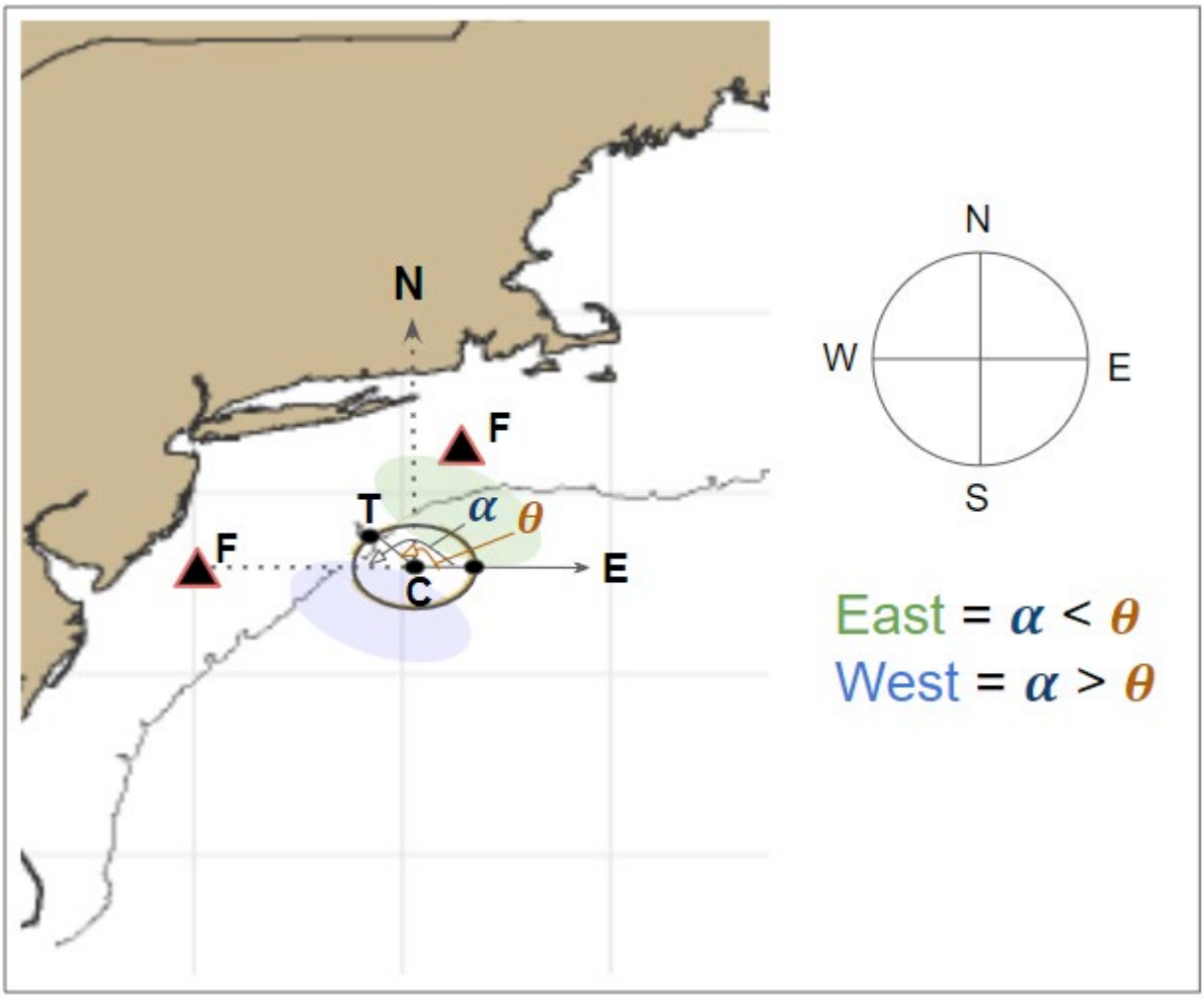

Figure 4. Generalized additive model (GAM) partial residual plots for variables with significant relationships to catch per unit effort (CPUE). Covariates are plotted against their splines (held constant) thus, the y-axis represents changes in CPUE (the response variable) relative to its mean following changes in the covariate. Smooths are presented in order of the strength of their relationship to CPUE: (a)latitude/longitude, (b) bottom temperature, (c) salinity at 222 meters depth (d) ring footprint index in zone 2, lagged by 6 months, (e) ring footprint index in zone 1, lagged by 3 months (f) standard deviation of sea surface temperature, (g) chlorophyll frontal dynamics.

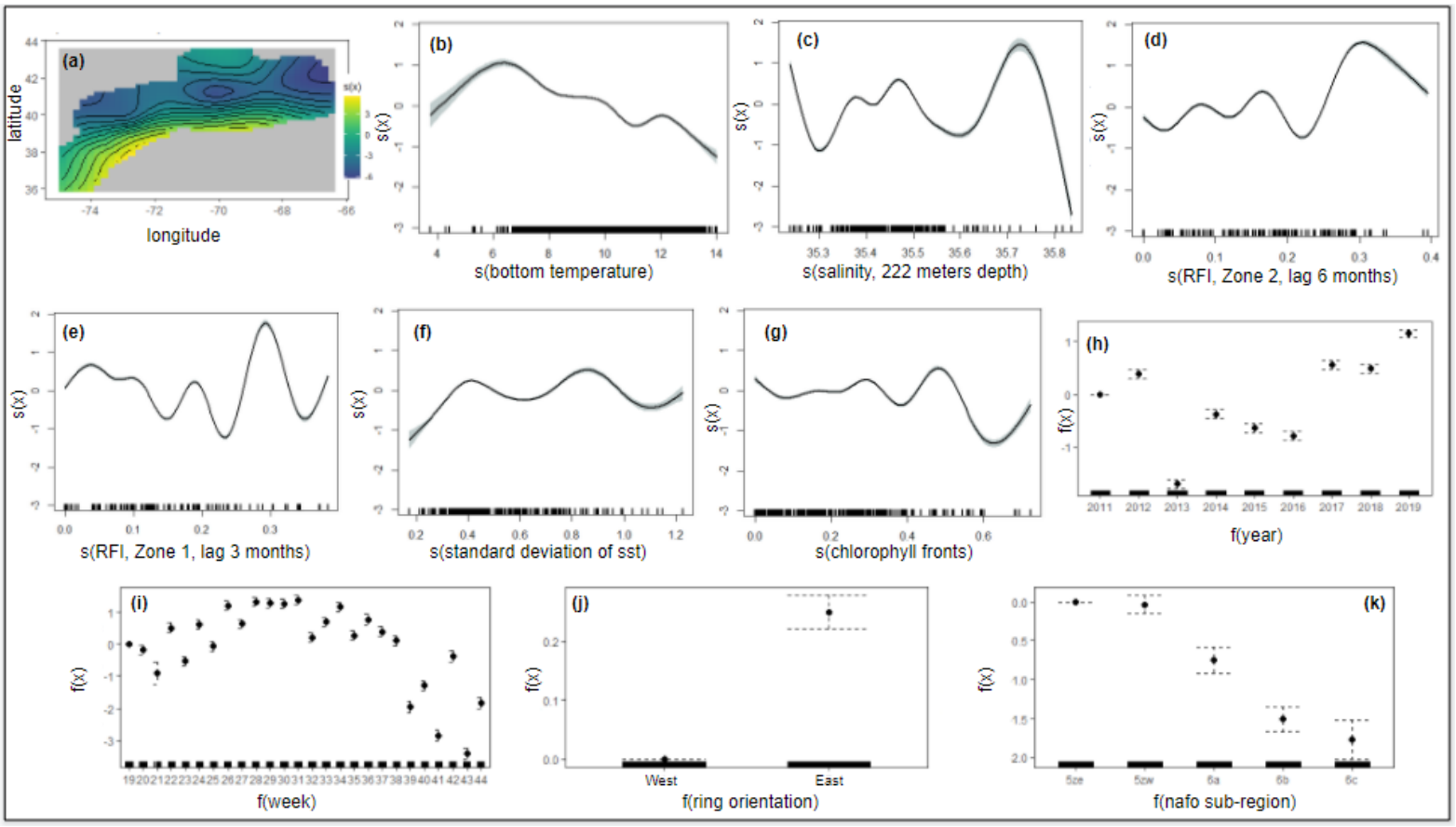

Appendix 1.

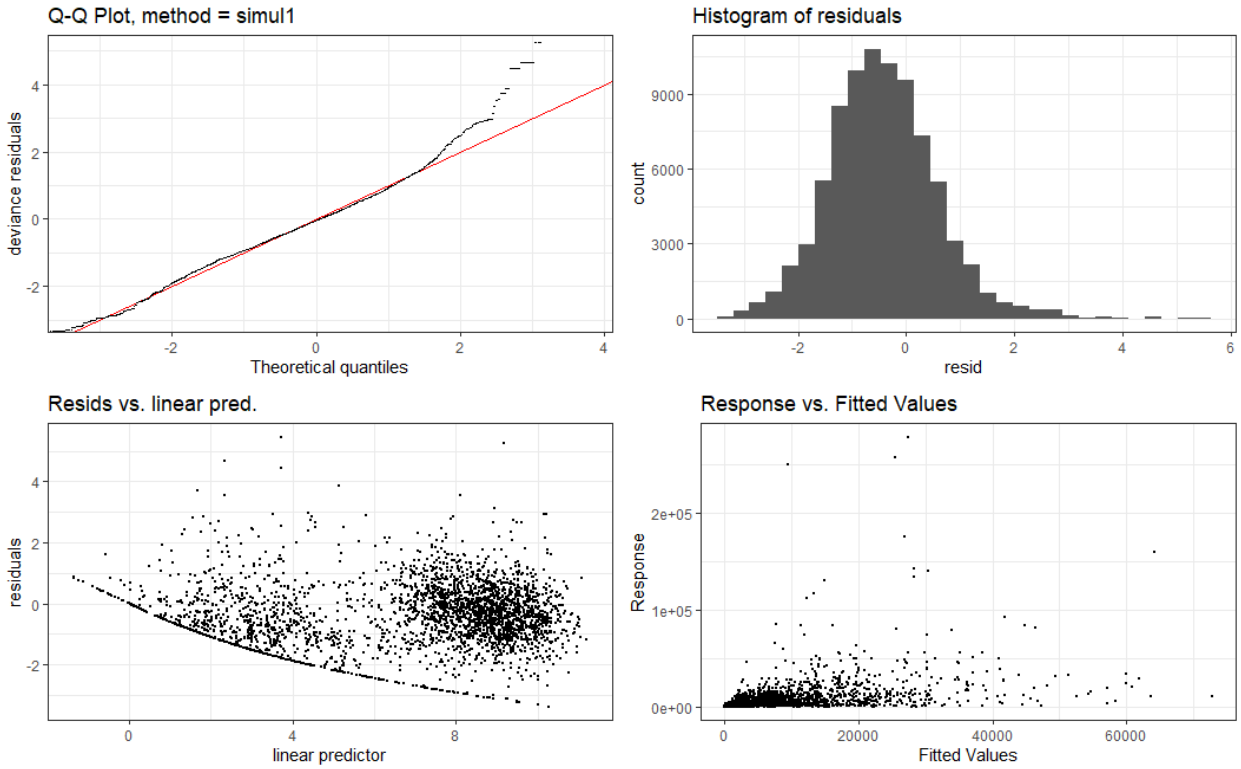
Q-Q Plot, method = simul1
deviance residuals
Theoretical quantiles
Histogram of residuals
count
resid
Resids vs. linear pred.
residuals
linear predictor
Response vs. Fitted Values
Response
Fitted Values

Appendix 2.

Family: Negative Binomial(0.629)

Link function: log

Formula:

cpue ~ as.factor(year) + as.factor(week) + s(lon, lat, k = 25) +
s(bt) + s(sal_222m) + s(z2lag6mo) + s(z1lag3mo) + s(sst_sd) +
s(fvalid_chl) + orientation + nafo_zone

Parametric coefficients:

	Estimate	Std. Error	z value	Pr(>|z|)
(Intercept)	6.82321	0.09734	70.096	< 0.0001
as.factor(year)2012	0.38388	0.04363	8.798	< 0.0001
as.factor(year)2013	-1.70563	0.03812	-44.739	< 0.0001
as.factor(year)2014	-0.38135	0.04165	-9.157	< 0.0001
as.factor(year)2015	-0.64601	0.04417	-14.626	< 0.0001
as.factor(year)2016	-0.79377	0.04684	-16.945	< 0.0001
as.factor(year)2017	0.56614	0.04441	12.749	< 0.0001
as.factor(year)2018	0.48686	0.03792	12.839	< 0.0001
as.factor(year)2019	1.15250	0.03688	31.253	< 0.0001
as.factor(week)20	-0.17665	0.07959	-2.219	0.02646
as.factor(week)21	-0.89393	0.18027	-4.959	7.09e-07
as.factor(week)22	0.50851	0.08320	6.112	9.85e-10
as.factor(week)23	-0.51258	0.07589	-6.754	1.44e-11
as.factor(week)24	0.61085	0.07391	8.265	< 0.0001
as.factor(week)25	-0.06688	0.07731	-0.865	0.38696
as.factor(week)26	1.18784	0.07396	16.061	< 0.0001
as.factor(week)27	0.63784	0.06914	9.226	< 0.0001
as.factor(week)28	1.32318	0.07081	18.687	< 0.0001
as.factor(week)29	1.27228	0.07501	16.962	< 0.0001

```
as.factor(week)30    1.26257    0.07557  16.708  < 0.0001
as.factor(week)31    1.37460    0.07468  18.406  < 0.0001
as.factor(week)32    0.21255    0.07642   2.781  0.00541
as.factor(week)33    0.68852    0.07360   9.355  < 0.0001
as.factor(week)34    1.16674    0.08069  14.459  < 0.0001
as.factor(week)35    0.25462    0.07512   3.390  0.00070
as.factor(week)36    0.76796    0.08196   9.370  < 0.0001
as.factor(week)37    0.39209    0.08227   4.766 1.88e-06
as.factor(week)38    0.10830    0.08547   1.267  0.20511
as.factor(week)39   -1.95255    0.08222 -23.747  < 0.0001
as.factor(week)40   -1.28605    0.08320 -15.457  < 0.0001
as.factor(week)41   -2.84740    0.08034 -35.442  < 0.0001
as.factor(week)42   -0.38399    0.08737  -4.395 1.11e-05
as.factor(week)43   -3.41932    0.08759 -39.039  < 0.0001
as.factor(week)44   -1.83128    0.09369 -19.546  < 0.0001
orientationS         0.24881    0.01438  17.306  < 0.0001
nafo_zone5zw        -0.03275    0.05929  -0.552  0.58072
nafo_zone6a         -0.74700    0.08351  -8.945  < 0.0001
nafo_zone6b         -1.50859    0.08423 -17.911  < 0.0001
nafo_zone6c         -1.77094    0.12805 -13.830  < 0.0001
---
Approximate significance of smooth terms:
               edf Ref.df Chi.sq p-value
s(lon,lat)  23.927 23.999  52952  <0.0001
s(bt)        8.895  8.997   2325  <0.0001
s(sal_222m)  8.983  9.000   3413  <0.0001
s(z2lag6mo)  8.976  9.000   4753  <0.0001
s(z1lag3mo)  8.994  9.000   3928  <0.0001
```

s(sst_sd) 8.804 8.988 1429 <0.0001

s(fvalid_chl) 8.964 9.000 1452 <0.0001

R-sq.(adj) = 0.222 Deviance explained = 69.9%

-REML = 5.8177e+05 Scale est. = 1 n = 83015